A Study on the Numerical Wave Propagation Properties of the Finite Difference-Time Domain(FD-TD) Method for EM Wave Problems

Ihn S. Kim *Regular Member*

전자파 문제에 대한 시간영역-유한차분법의 수치파 전파모델의 성질에 관한 연구

正會員 金 仁 顥*

ABSTRACT

In this paper, the numerical wave propagation properties of the finite difference-time domain (FD-TD) method is investigated as a discrete model describing electromagnetic(EM) wave propagation phenomena. The leap-frog approximation of Maxwell's curl equations in time-space simulates EM wave propagation in terms of the numerical characteristic and the domain of dependence. A geometrical interpretation of the FD-TD numerical procedure is presented. The numerical dispersion error due to the leap-frog approximation and its dependence on the stability factor are illustrated. The FD-TD method using the leap-frog approximation is inherently a descriptive model. Thus, not only any physical picture about EM wave propagation phenomena can be drawn through this model, but also physical or engineering parameters in the frequency domain can be extracted from descriptive results. E-plane filter characteristics in the WR-28 rectangular waveguide and reflection property of an inductive iris in the WR-90 rectangluar waveguide extracted from simulation of the FD-TD model is included.

要 約

본 논문에서는 전자파의 전파현상의 불연속모델로서 시간영역-유한 차분법의 수치적 성질이 연구된다. 시간-공간의 차원에서 막스웰 방정식을 개구리뜀 근사식으로 나타내므로 수치적인 특성과 의존 영역의 항으로 전자파의 전파현상을 모사한다. 시간영역-유한차분법의 수치직모사과정이 기하하적으로 설명된다.

개구리뜀 근사법의 채용으로 인한 수치적인 분산현상이 예시된다. 개구리뜀 근사법은 기초로 한 시간영역 -유한차분법은 원래계산 결과만을 산출하는 모델이 아니고 묘사적인 모델이므로 전자파 전파현상에 대한 물리적인 현상을 묘사할 뿐만 아니라 이러한 묘사적인 결과로부터 푸리에 변환을 통하여 주파수 영역에서 의 결과를 추출할 수 있는 매우 유연한 수치해석 방법이다. 그래서 본 수치해석 방법을 이용하여 WR-28 과 WR-90 도파관의 E-평면 필터와 인덕티브 아이리스의 특성분석 결과를 포함시킨다.

I. Introduction

Propagation problems are one among three ma jor categories of problems (equilibrium, eigenval ue, and propagation problems) in physis and en gineering[1]. Electromagnetic(EM) wave scat tering phenomena belong to this category. Pure propagation phenomena are modeled with Max well's two time depedent curl equations without any source or dissipative terms. Thus, it is well known that the time dependent curl equations are an analytical model(physical law) of EM wave propagation since the analytical model mothem atically simulates real propagation of fields in con tinuous media.

Numerical computational methods in time do main are playing an increasingly important role in the solution of EM problems, since they can si mulate, albert in discretized form, physical phen omena as they evolve in nature. Many people consider simulation to be a mere computational technique yielding engineering parameters, since frequency domain techniques have been dominan tly used to calculate not physical processes, but rather engineering parameters. Even though nu merical simulation is one branch of the broader area of computational electromagnetics, we like to distinguish it from the purely computational electromagnetics, which employs prescriptive mo dels to predict specific engineering parameters. Simulation methods are descriptive models, with which physical processes can be described and visualized.

The finite difference-time domain(FD-TD) meth od using the leap-frog scheme has been mostly used in the prescriptive way to calculate particu lar engineering parameters of EM problems [2]

[14]. The FD-TD approach is actually a more powerful numerical method for simulating EM wave propagation phenomena. We study wave propagation in a rectangular waveguide structure in order to provide physical insight into the pro cess. In this way, the FD-TD process can be bet ter understood, and more light is shed on the property of continuous Maxwell's equations as well. Futhermore, since the simulation method yields physical pictures of propagation phenom ena, it allows us to perform visual experiments even though we must still rely heavily on heuris tic reasoning, physical intuiton, and trial-and-er ror procedures. Many experiments can be carried out with complete freedom from certain physical constraints, since boundary conditions are simply specified by numbers. Futhermore, when probing (sampling) field quantities within a computational domain, the system is not perturbed.

The behaviour of the leap-frog approximation in a time-space grid structure resembles that of the continuous model. Thus, discrete numerical wave motion can be interpreted in analogy to the continuous wave propagation phenomenon. The concept of numerical characteristics and domain of dependence were first introduced by Courant, Friedrich, and Lewy(CFL) for a simple hyper bolic partial differential equation in their import ant paper [14]. By using these concepts, we de velop in Section 3 and 4 the leap-frog approxi mation as a local wave propagation model in dis crete time-space coordinates, and provide some geometritical interpretation of the numerical pro cess.

The discrete approximation creates a numerical dispersion error which depends on the mesh size to wavelength ratio. The standard way of analy

zing the distortion of a propagating wave is to study its dispersion relation. The dispersion characteristics of the FD-TD method have been analyzed by Taflove[16]. The effect of the stability factor on the numerical dispersion has been demonstrated by the author [17] and [18]. These characteristics and the effect will be described in Section 5.

A series of qualitative observations on how wave propagates in a standard rectangular waveguide has been made. The observation and calculation results of engineering parameters can be found in Section 6.

This paper starts with a review of mathematical solution methods for Maxwell's equations in hyperbolic differential equation form in the next section. Discrete solution methods such as the leap-frog approximation of Maxwell's curl equations have been extensively dealt with in the literature [2], [3], [6], or [11].

II. Mathematical Review

The analytical solution methods of Maxwell's two time dependent curl equations are studied in this section. In order to study a pure EM wave propagation model, Maxwell's curl equations are considered without any source and dissipative terms. They are in matrix form:

$$\frac{\partial}{\partial t} \begin{vmatrix} \bar{E} \\ \bar{H} \end{vmatrix} = \begin{vmatrix} 0 & 1/\varepsilon \\ -1/\mu & 0 \end{vmatrix} \cdot \begin{vmatrix} \triangledown \times & 0 \\ 0 & \triangledown \times \end{vmatrix} \cdot \begin{vmatrix} \bar{E} \\ \bar{H} \end{vmatrix} \tag{1}$$

or in compact notation:

$$\frac{\partial \bar{U}}{\partial t} = \bar{A} \cdot \bar{L} \cdot \bar{U} = \bar{A} \cdot \frac{\partial \bar{U}}{\partial R} \tag{2}$$

where

$$\bar{U} = \begin{vmatrix} \bar{E} \\ \bar{H} \end{vmatrix},$$

$$\bar{A} = \begin{vmatrix} 0 & 1/\varepsilon \\ -1/\mu & 0 \end{vmatrix},$$

$$\bar{L} = \begin{vmatrix} \triangledown \times & 0 \\ 0 & \triangledown \times \end{vmatrix},$$ and R is a position vector.

Maxwell's equations describe total field quantites, $\bar{E}$ and $\bar{H}$:

$$\bar{E} = \bar{E}^s + \bar{E}^i,$$

$$\bar{H} = \bar{H}^s + \bar{H}^i,$$

where the superscripts s and i indicate the scattered and incident fields.

Propagation problems are mathematically treated as initial value problems in free boundaries that have an unsteady or transient nature. If a boundary value problem is added to an initial value problem, then in mathematical parlance, such a problem is known as initial boundary value problem or mixed initial value boundary value problem. All EM wave scattering problem belong to this class. The solution method for initial boundary value problems[1] is briefly described below. If the initial condition of U is

$$\bar{U}(\bar{R}, t = 0) = f(\bar{R}) \tag{3}$$

and the boundary condition is

$$\bar{U}(\bar{R}, t) = \bar{g}(\bar{R}, t), \qquad t \geq 0 \tag{4}$$

then the solution is

$$\bar{U}(\bar{R}, t) = f(\bar{R} \pm ct) \tag{5}$$

where of course $\bar{f}(0)$ must be equal to $\bar{g}(0, 0)$. Two solutions for a pulse propagation are shown in Figs. 17(a)-(i), where the pulse excited in the middle of waveguide is split into two solutions like (5), a wave moving to the left and the other wave moving to the right.

Fig. 1 illustrates the general initial boundary value problem[1] as follows. The value of the vector U at some point x(space vector) at later times is determined entirely by the data on the
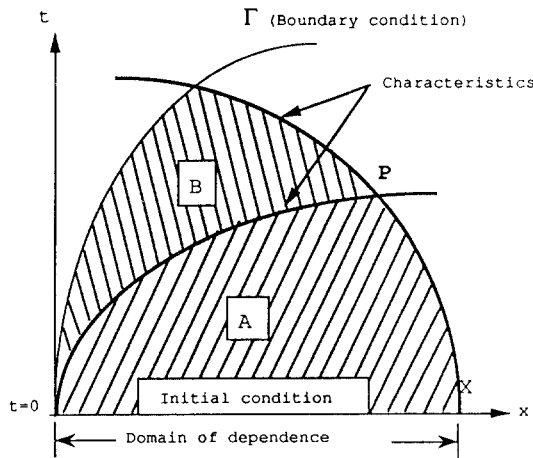
1597

Fig. 1. Graphical representation of the general initial boundary value probelm

segment of the initial line lying between the out most characteristics drawn backward from the point p to the initial line. This segment is called the domain of dependence of the point p. The situation is shown in Fig. 1 for the one-dimensonal case. It is known that the solution in the region A, enclosed by the characteristics, is determined by the initial condition and that the extension of solution into region B is determined by the boundary condition. More generally, the number of unknown component of U that can properly be prescribed on a curve Γ is equal to the number of characteristics entering region B from Γ. In propagation problems, therefore, the solution marches out from the initial state guided and modified in transit by the boundary conditions.

Characteristics are the lines in the plane of the independent variables along which waves(signals) can propagate. In a source free case, characteristics of Maxwell's equations are the same as those of the homogeneous wave equation. The characteristics produce a conical surface in two space dimensions as shown in Fig. 2. The conical domain Ω in the two space dimensions becomes the interval AB (circle) on the x-axes from the apex (x^{0}, t^{0}). The value of U at (x^{0}, t^{0}) depends only

on the values of U and U_t(The subscript t indicates a derivative with respect to time t.) on the interval AB(circle) and this interval is the domain of dependence of the solution at (x^{0}, t^{0}). Thus the points A and B (or circle) represent the position of a wavefront in space as a function of time in EM wave propagation. Maxwell's two time dependent curl equations possess two families of real characteristics like the wave equation : one describes forward traveling waves and the other backward traveling waves. Physical systems that are governed by Maxwell's two time dependent curl equations are ones in which waves (signals) propagate at a finite speed (speed of light) in a finite region as :

$$(x_1 - x_{01})^2 + (x_2 - x_{02})^2 = (ct)^2 \tag{6}$$

In the one space dimensional case, the lines of PA = constant and PB = constant represent the two families of characteristics along which the wave (signal) propagates. An observer at point P is subject to the effects of what has happened in the crosshatched region, AB, but disturbances outside this region cannot be felt. This region is known, therefore, as the domain of dependence at point P. Similarly, a disturbance created at point P can be felt only in the vertically crosshatched region known as the domain of influence. The functional analogy of the domain of dependence in this continuous case will be used to interpret numerical (FD-TD) wave propagation characteristics in a discretized computational domain in the next section. As mentioned in the beginning of this section, it is recommended to see other references, for example [2] or [3], for finite difference equation aspects.

III. Local Wave Propagation Model

The leap frog approximation is shown as a local propagation model for the FD-TD approach simulating EM wave propagation phenomena in this section. This illustration is based on the analogy

of the numerical characteristic and domain of dependence which Courant et. al. introduced in their important paper [14] in 1951. They made an analogy between continuous characteristic and domain of dependence (of simple hyperbolic partial differential equation) and numerical characteristic domain of dependence (of one-dimensional finite difference equation). We have observed a relationship between both features. We first introduce the one-dimensional view of the numerical characteristics and allows us to analyze only TEM propagation. Then, comparative pictures for the two cases in two space dimensions are presented in Fig. 4 and 5.

Figure 3 shows the domain of dependence for the finite differenced equation and the basic leap-frog scheme in one space dimension. The point Q at time level $(n+1)\triangle t$ is calculated from the points A, B, D on time levels $(n+1/2)\triangle t$ and $n\triangle$ t, which have in turn been calculated from C, D, E, G, H, L on $n\triangle t$ and $(n-1/2)\triangle t$, etc. Clearly the numerical domain of dependence of the point Q is limited by QCJ and QEN. The physical domain of dependence of Q is limited by the extreme characteristics J and N through Q. The extreme characteristics are determined by the upper limit value of the stability inequality.

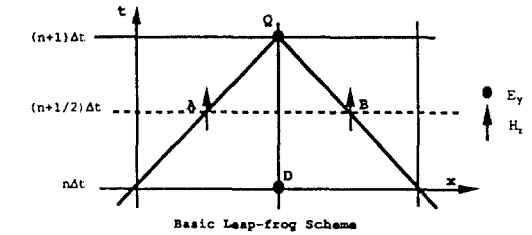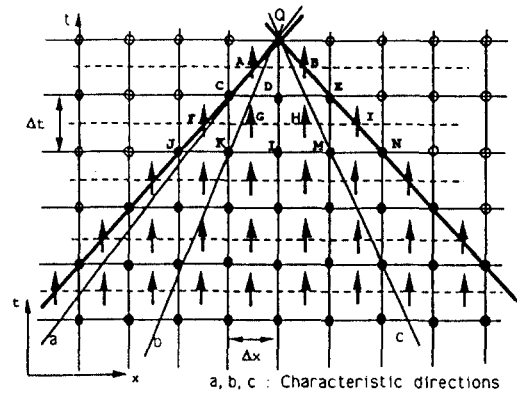a, b, c : Characteristic directions

Basic Leap-frog Scheme

Fig. 3. Numerical characteristics and domain of dependence on the time-space grid structure.
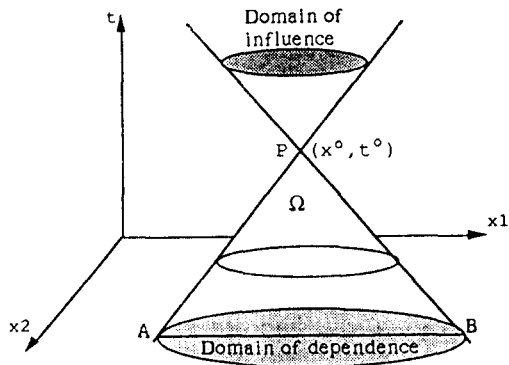

Fig. 2. Forward and backward characteristic cones with apex at P and domain of dependence of Maxwell's two time dependent curl equations.
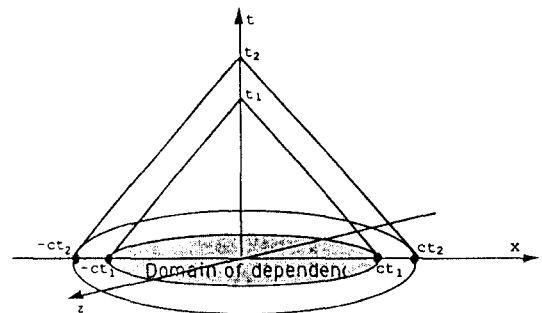

Fig. 4. Characteristic cones and domain of dependence for the two space dimensions at time steps t_1 and t_2.

1599

To obtain a convergent and thus stable calcu
lation, it is necessary that any pertubation that
can influence Q physically must also be able to do
this numerically(the discretization may not cut
off physically possible influences). This requires
the physical domain of dependence to be conta
ined completely in the numerical domain of de
pendence. The slope of the characteristics leads
to the CFL stability condition which will also be
described in the next section. The characteristics
and the domain of dependence play an important
role in the analysis of wave propagation phenom
ena.

For the 2-D case, the characteristics cones of
the continuous model in two space domensions at
two specific times t_1 and t_2 are shown in Fig. 1.
For the leap-frog approximation, a local wave mo
tion based on TE mode propagation is illustrated
in the discrete time-space mesh structure as shown
in Fig. 5 where the H field components are placed
at the points F, G, I and K, which are on the
characteristic lines (AP_1, BP_1, CP_1, and DP_1) at
the half time steps on the half space intervals.
For a local wave motion based on TE mode propa
gation in the discrete domain, we illustrate the
2-D leap-frog approximation in the time-space grid
structure. This is shown in Fig. 5. The leap-frog
scheme in Fig. 5 shows that H field values at the
points F, G, I, and K at a time step $(n+1/2)\triangle t$
are dependent upon the E field values at A, B, C,
D, and P at a time $n\triangle t$. And the E field value at
the point P_1 at a time $(n+1)\triangle t$ is updated by
using the H field values at the points F, G, I, and
K at a time $(n+1/2)\triangle t$ and the E field value at
the point from the previous time step $n\triangle t$. The
discrete characteristics of the leap frog approxi
mation for a time step form a square in a compu
tational domain since a uniform mesh size is em
ployed, otherwise a rhombus is generally formed,
with the four points A, B, C, and D for the E
fields and F, G, I, and K for the H fields. This
square behaves like the domain of dependence in
the continuous case[15]. It is obvious that in the
three-dimensional (x, y, t) mesh structure the

characteristics of the differential equations are
circular cones, whereas those of the differenced
(leap froged) equations are four-sided pyramids
on the square. But in the four-dimentional (x, y,
z, t) mesh structure, the characteristics of the
leap-forg approximation form a four-sided pyra
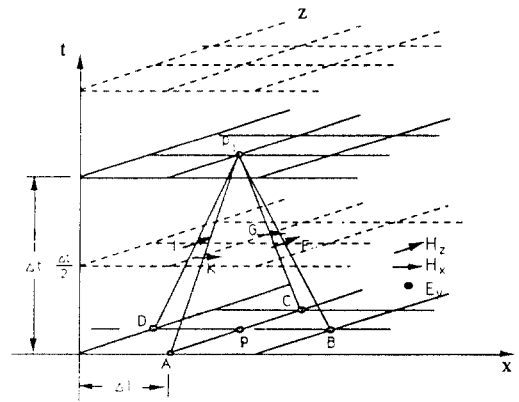mid on every surface of a cube.

Fig. 5. Three dimensional (x, y, t) diagram showing
the characteristic of the leap frog approximation
for TE mode propagation.

Ⅳ. Geometrical Interpretation

Projections (circles) of the domain of dependence
for continuous propagation are shown in the dis
cretized computational domain as the projections
(squares) of the discrete domain of dependence
on the two-space plane in Fig. 6. The square are
domains of dependence for the leap-frog approxi
mation. The CFL stability condition for the dif
ferenced equations states that in order to be con
vergent for all smooth initial data, the square of
dependence of the difference equations must con
tain completely the circle of dependence of the
differential equations. There is no loss of gener
ality if we consider the grid point O to lie on the
t-axis at $x = x_0$ and $z = z_0$. If $T = n\triangle t$, then the
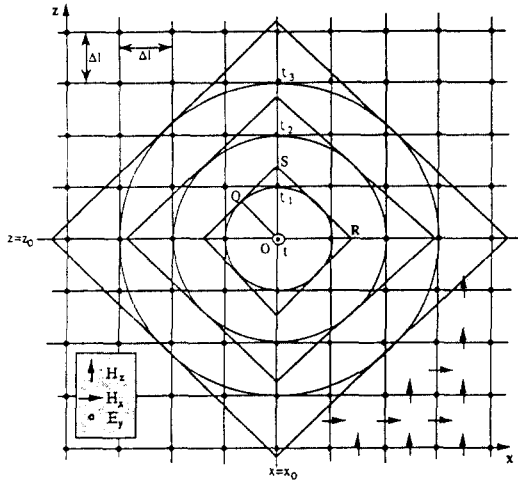domain of dependence for the differential equa-

Fig. 6. Projections of the characteristic circles and squares (propagation behaviour) in the space plane (x, z)(domain of dependences) at time steps t_1, t_2, and t_3.

tion is given by

$$x_n^2 + z_n^2 \leq n^2 \triangle t^2 \tag{7}$$

and so in Fig. 6, $OQ = n \triangle t$ where n is 1. Now the square of dependence for the difference equation, shown in Fig. 6, has $OR = OS = n \triangle l$ where n is 1, and so the CFL condition is satisfied provided the square includes the circle, and this is the case [15] if

$$c \cdot n \cdot \triangle t \leq \frac{1}{\sqrt{2}} \cdot n \cdot \triangle l, \tag{8}$$

or

$$\frac{c \cdot \triangle t}{\triangle l} \leq SF \tag{9}$$

where c is the speed of light, $SF = \sqrt{\dfrac{\varepsilon_r \mu_r}{2}}$ is the stability factor, n is the number of iterations. This confirms the stability inequality given by Courant [14] and Von Neumann [15].

As the circles are interpreted as wavefronts at given instants in the continuous case, the squares are wavefronts in the discrete case. Since the normal of wavefronts points into the propagation direction, the numerical wavefront at the propagation direction $45°$ in the uniform mesh corresponds to the wavefronts of the continuous model as shown in Fig. 6. And, as the angle of propagation direction changes, i.e., from the direction of OQ to the axial direction, the difference between two cases is increased. No difference between numerical and continuous case at the propagation angle $45°$ will be noticed when analyzing the numerical dispersion in the next section.

The value of the stability factor can be considered as a proportionality coefficient which controls the propagated distance in the discrete computational domain since the stability factor provides a normalized distance vector on the grid structure. So, the maximum propagated distance is determined by the maximum value of the stability factor which provides the maximum $\triangle t$. This can be explained with a forerunner. As the value of the stability factor is increased, the effect of forerunner is also increased. Thus, how the numerical wave propagates in a uniform meshed domain can be predicated with (8). If SF is zero, then the numerical wave is stationary, i.e., does not propagate at all. Some value close to zero require a large number of iterations.

This effect of the stability factor must be included in the Fourier transform as follows :

$$s(f) = \sum_{n=1}^{N} S_n(i_0, j_0, k_0) e^{-j2\pi \cdot n \cdot f \cdot SF} \tag{10}$$

where s is spectrum, S is the time domain sample, n is the iteration number, (i_0, j_0, k_0) is the sampling position in the computational domain, and f is the frequency measured in cycles per sampling interval.

V. Numerical Dispersion Relation

The standard way of analyzing the distortion of a propagating wave is to study its dispersion re-

1601

lation. The numerical discretization of Maxwell's equations produce a numerical dispersive phenomenon that is different from the physical dispersion phenomena. As its name indicates, this numerical artifact causes the phase velocity to become a function of the mesh size. A wave propagating in a discrete mesh becomes progressively dispersed with increasing travel time. Hence, numerical dispersion is a significant problem in the method and thus its effect must be reduced as much as possible. To see the dispersion effects of the numerical approximation, we will analyze dispersion characteristics in a region away from any boundary in order to avoid boundary effects. The velocity is also a function of the stability factor. Numerical dispersion characteristics have been studied in [16]. The dispersion relation for the 3-D leap-frog approximation in a uniform mesh is given by

$$\sin^2\left(\frac{\omega \triangle t}{2}\right) = SF^2\left[\sin^2\left(\beta_x \frac{\triangle l}{2}\right) + \sin^2\left(\beta_y \frac{\triangle l}{2}\right) \right.$$
$$\left. + \sin^2\left(\beta_z \frac{\triangle l}{2}\right)\right] \qquad (11)$$

where β_x, β_y, and β_z are x−, y−, z− components of the wave number, and

$$SF = \frac{v_{ph} \triangle t}{\triangle l} \leq \sqrt{\frac{\varepsilon_r \mu_r}{n}} .$$

We know that the continuous dispersion relation in free space (no dispersion) is

$$\beta_0^2 = \frac{w^2}{c^2} = \beta_x^2 + \beta_y^2 + \beta_z^2 \qquad (12)$$

As $\triangle x$, $\triangle y$, $\triangle z$, and $\triangle t$ go to zero, (11) reduces to (12). This means that the dispersion increases as the mesh size $\triangle l$ becomes larger. For TE mode propagation in the two dimensions, (11) reduces to

$$\sin^2\left(\frac{\omega \triangle t}{2}\right) = SF^2\left[\sin^2\left(\frac{\beta \cdot \cos\theta \cdot \triangle l}{2}\right) \right.$$
$$\left. + \sin^2\left(\frac{\beta \cdot \sin\theta \cdot \triangle l}{2}\right)\right] \qquad (13)$$

where θ is the propagation angle with respect to the positive x-axis. Equation (13) is further reduced for the normalized phase velocity as

$$\frac{v_{ph}}{c} = \frac{\lambda_0}{SF \cdot \pi \cdot \triangle l} \sin^{-1}$$
$$\left[SF \sqrt{\sin^2\left(\frac{\pi \cdot \triangle l \cdot \cos\theta}{\lambda_0}\right) + \sin^2\left(\frac{\pi \cdot \triangle l \cdot \sin\theta}{\lambda_0}\right)}\right] \qquad (14)$$
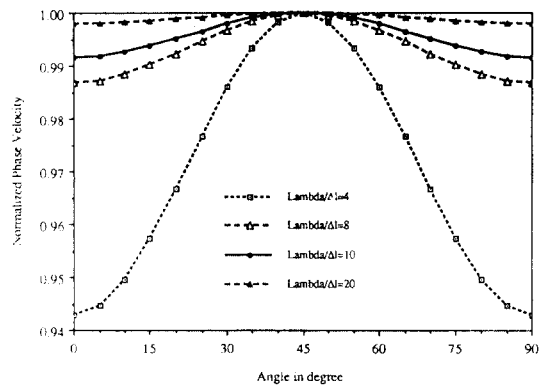

Fig. 7. Numerical dispersion characteristics for various mesh sizes at $SF = \frac{1}{\sqrt{2}}$.
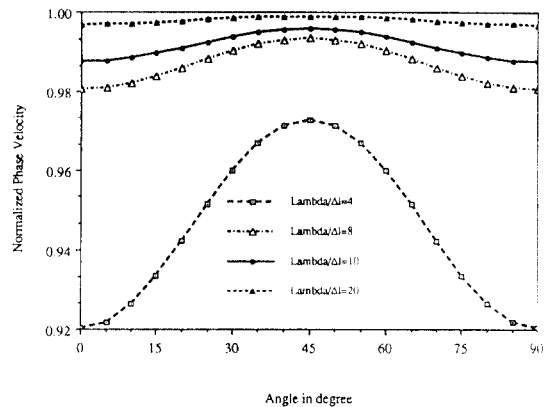

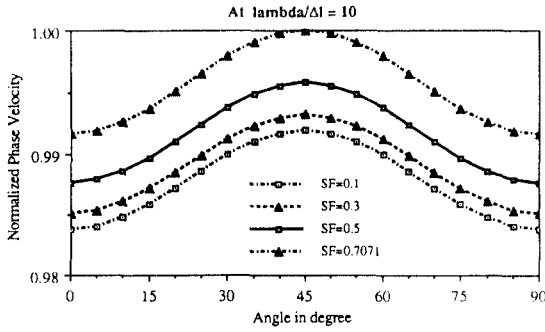Fig. 8. Numerical dispersion characteristics for mesh sizes at $SF = 0.5$.

Fig. 9. Numerical dispersion characteristics for various values in the stability inequality.

The normalized phase velocity, (14), is plotted as a function of the propagation angle for four different mesh sizes at $SF = 1/\sqrt{2}$. This is shown in Fig. 7 where the unity of the normalized phase velocity indicates no dispersion at all. Fig. 8 demonstrates the same characteristic as $SF = 0.5$ as shown in [16]. By comparing the two figures, Figs. 7 and 8, the smaller numerical dispersion error is shown at $SF = 1/\sqrt{2}$ rather than at $SF = 0.5$ for the two-dimensional case. For the mesh size, $\lambda_0/\triangle l = 10$, and any propagation angle in the mesh the maximum dispersion error predicted for $SF = 1/\sqrt{2}$ is 0.837%, whereas for $SF = 0.5$ the maximum dispersion is 1.24%.

Fig. 9 illustrates the effect of the stability factor on the numerical dispersion error if the mesh size is $\lambda_0/\triangle l = 10$. A comparison of the dispersion property at four different values of the stability factor (0.1, 0.3, 0.5, and $1/\sqrt{2}$) means that the upper limit of the stability inequality would yield the least velocity error due to numerical dispersion for a given mesh size.

From Figs. 7, 8 and 9, it is observed that the numerical phase velocity is maximum at a propagation angle of $45°$ and minimum at angles of $0°$ and $90°$ for any mesh size. We can see from Fig. 7 that only at $45°$ the discrete propagation characteristic meets that of the continuous propagation as described in the last section. This agrees with the above dispersion analysis. The numerical dis-

persion also cause the higher frequency components to be delayed relative to the lower frequency components and thus substantial tailing of the signal arises [16]. In order to keep the dispersion error less than 0.5% in the 2-D case, $SF = 1/\sqrt{2}$ and a minimum mesh parameter of $\lambda_0/13$ must be employed in the program formulation. Fig. 9 suggests that upper limit of the stability inequality in [17] will ensure lowest dispersion error and smallest number of iterations.

In addition to being dependent upon frequency, the propagation velocity of the numerical solutions is also dependent upon direction. This property is called the numerical anisotropy resulting only from the space discretization, not from the time discretization. This occurs in the numerical approximation of hyperbolic equations in two space dimensions, but not in one-dimensional cases. This error depends also on the number of $\triangle l$ per wavelength, and is minimized by increasing the number of mesh elements per shortest wavelength ($\lambda/\triangle l \geq 12$ for less than 0.5%) in the simulation. The derivation for TE modes agrees with the analysis of the numerical dispersion relation. For a uniform mesh and the leap-frog approximation, the numerical phase velocity, c^*, associated with the space discretization can be obtained with

$$\frac{c^*}{c} = [\sin^2(\beta\triangle l \cdot \cos\theta)\cos^2(\beta\triangle l \cdot \sin\theta)$$
$$+ \sin^2(\beta\triangle l \cdot \sin\theta)\cos^2(\beta\triangle l \cdot \cos\theta)]^{\frac{1}{2}} \qquad (15)$$

where θ is the propagation direction with respect to the x axis. Note that if $\beta\triangle l \to 0$, then $c^* \to 0$. A polar diagram representing the normalized phase velocity c^*/c as a function of $\beta\triangle l$ and the propagation direction θ is shown in Fig. 10. Note that the anisotropy error could be almost neglected if a wavelength is resolved by more than $8\triangle l$.

Since errors due to numerical dispersion are introduced by the leap-frog approximation of Maxwell's equations, the numerical group velocity error must also be considered. The group velocity
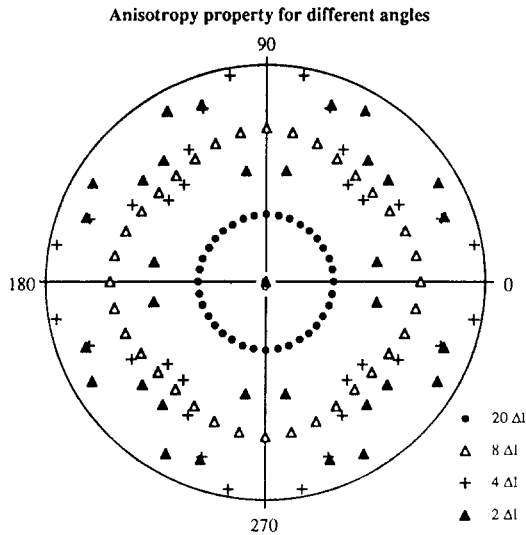
1603

Anisotropy property for different angles

Fig. 10. The anisotropy is represented in a polar dia
gram for four different mesh sizes. Note that
amplitudes are not related to each other

indicates the speed and direction of the propa-
gation of the energy contained in the spectral
component of a wave packet or wave group. En
ergy is used here in the general sense of a quan-
tity proportional to the amplitude of the variable
squared. For dispersive waves, the group velocity
differs from the phase velocity and is perhaps a
more important quantity to examine in an error
evaluation than the phase velocity. The CFL sta
bility condition also governs the numerical group
velocity. As in the numerical phase velocity case,
the numerical group velocity error is minimum at
the upper limit of the stability inequality as will
be shown later in this section.

The group velocity, $v_g = d\omega/d\beta$, is derived from
the dispersion relation (11) and is

$$v_g =$$

$$\frac{SF \sqrt{\sin^2(\beta \triangle l \cdot \cos\alpha_x) + \sin^2(\beta \triangle l \cdot \cos\alpha_y) + \sin^2(\beta \triangle l \cdot \cos\alpha_z)}}{\sin(\omega \triangle t)}$$

$$(16)$$

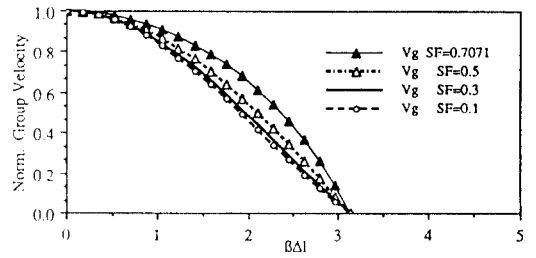where SF is the stability factor and α_x, α_y, and α_z

Fig. 11. Comparison of the group velocity error at the
propagation angle ($0°$ or $90°$) for various values
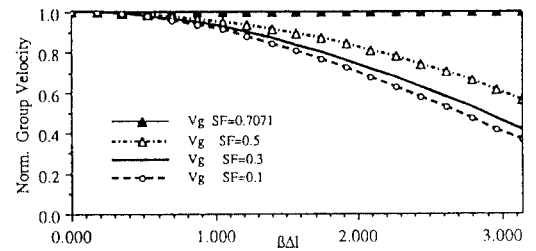of the stability factor.

Fig. 12. Comparison of the group velocity error at the
propagation angle ($45°$) for various values of
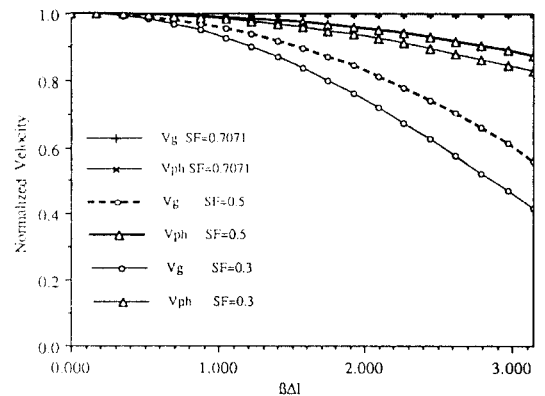the stability factor.

Fig. 13. Comparison of the phase and the group ve
locity errors at the propagation angle ($45°$) for
various values of the stability factor.

1604

are the wave propagation angles with respect to the coordinates x, y, and z respectively.

In Fig. 11, the numerical group velocity characteristic at propagation angles $0°$ or $90°$ (along the mesh) versus $\beta \triangle l$(radian) is shown for different values of the stability factor. This characteristic again suggests the use of a value close to the upper limit of the stability inequality. Another point is that the group velocity will be zero at $\beta \triangle l = \pi$ which corresponds to a wavelength $2 \triangle l$ in axial direction. This is directly related to the Nyquist sampling criterion for the minimum case.

In Fig. 12, the group velocity characteristic at a propagation angle $45°$, (diagonal in the mesh) as a function of $\beta \triangle l$(radian) is illustrated for four different values of the stability factor. This figure shows that the group velocity is faster for a propagation angle of $45°$ than that at $0°$ of $90°$. In particular, no group velocity error occurs at the upper limit of the stability inequality. This again comfirms that the local FD-TD wave propagates in the discretized computational domain along a direction determined by vectorial sum of the values along the unit cell as mentioned in the previous section.

In Fig. 13, a comparison between the group and the phase velocity characteristics at a propagation angle of $45°$ (diagonal), with respect to $\beta \triangle l$ is illustrated of three different values of the stability factor. It shows that no velocity error(for both the group and the phase velocities) occurs at the upper limit of the stability inequality. This comparison also illustrates that the group velocity is always slower than the phase velocity. As a result, both of the velocity error increase as the value of the stability factor decreases.

VI. Observations

In this section, a qualitative view of how a numerical wave propagates in a standard rectangular waveguide is presented. TE_{10} mode propagation has been simulated for both CW and pulse cases. Four different simulations of numerical wave
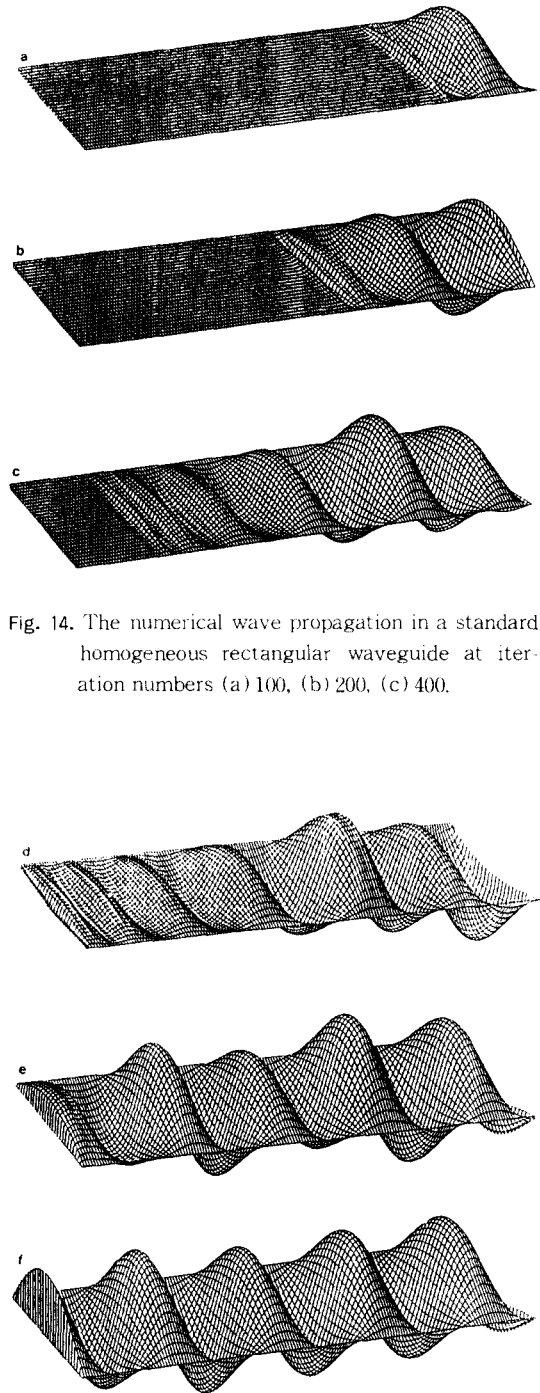

Fig. 14. The numerical wave propagation in a standard homogeneous rectangular waveguide at iteration numbers (a) 100, (b) 200, (c) 400.

Fig. 14. The numerical wave propagation in a standard homogeneous rectangular waveguide at iteration numbers (d) 500, (e) 800, (f) 1700.
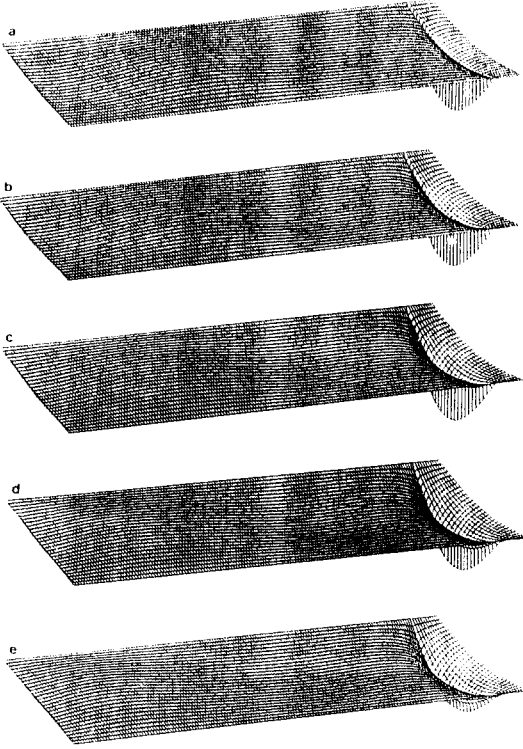
1605

Fig. 15. The numerical wave propagation below cutoff in a standard homogeneous rectangular wave guide at iteration numbers (a) 1886, (b) 1891, (c) 1896, (d) 1901, and (e) 1906.

propagation have been examined : i) without discontinuity, ii) with discontinuity, iii) below cutoff frequency, (these three use CW excitation), and iv) pulse excitation without any discontinuity. For all four cases, a matched boundary condition was placed at the left and right ends of the rec tangular waveguide, and an electric wall bounda ry condition is placed at the top and bottom of the domain.

E_y components were sampled and plotted in a 3 D graphical mode for each case. The CW case is illustrated first. Its excitation was of the form

$$E_y(i, k, n \cdot \triangle t) = \cos(\omega \cdot n \cdot \triangle t) \sin \frac{\pi(i-1)}{NX},$$
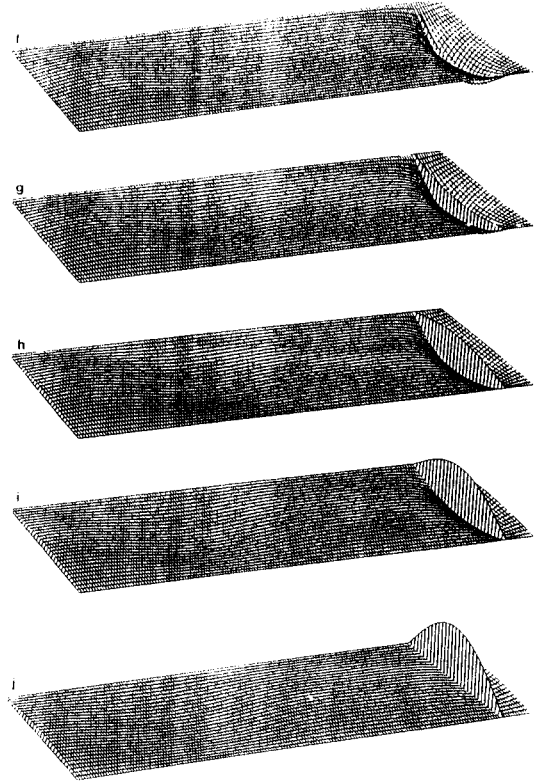$$(17)$$

Fig. 15. The numerical wave propagation below cutoff in a standard homogeneous rectangular wave guide at iteration numbers (f) 1911, (g) 1916, (h) 1921, (i) 1926, and (j) 1931.

where NX and (i, k) are respectively, the number of segments $\triangle l$, node points in x and z directions in the waveguide, and n is the number of time step. The size of the computational domain was $21 \triangle l$ in the z direction and $340 \triangle l$ in the k direction. The input signal was applied at $z = 10$ for each CW case.

The numerical wave propagation in an homogeneous rectangular waveguide was observed at 6 different iteration numbers : 100, 200, 400, 500, 800, and 1700. The snapshots at those iteration numbers are shown in Figs. 14(a)-(f). We observe that the wave propagates from the right to the left hand side. The forerunners to the wave front of the propagating wave have much smaller
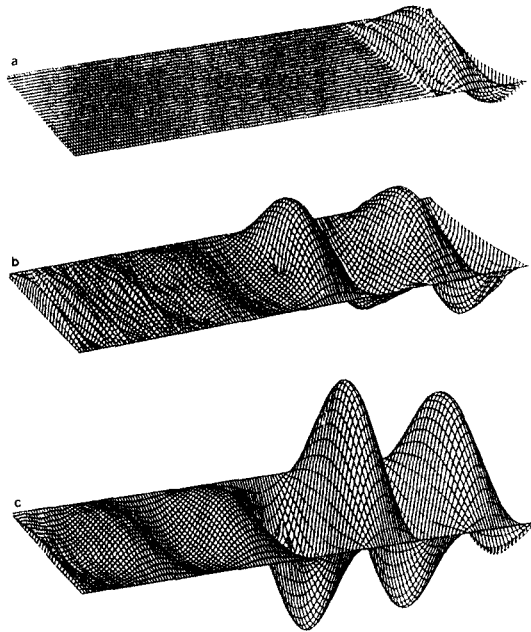
Fig. 16. The numerical wave propagation in a standard homogeneous rectangular waveguide with an obstacle at iteration numbers (a) 100, (b) 500, (c) 800.
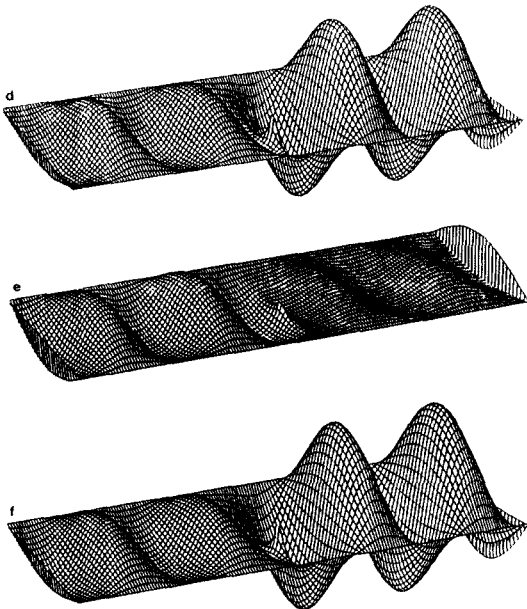

Fig. 16. The numerical wave propagation in a standard homogeneous rectangular waveguide with an obstacle at iteration numbers (d) 1000, (e) 1200, (f) 1900.

amplitudes than the wavefront as can be seen in Figs. 14 (a), (b), (c), and (d). In Fig. 14(f), we can see that a steady state condition has been reached.

A numerical simulation below cutoff can be observed in the snapshots of the E field plotted in Figs. 15(a)-(j). The WR-28 waveguide was excited with a signal of frequency 16 GHz. Observations were made for the iteration numbers 1886, 1891, 1896, 1901, 1906, 1911, 1916, 1921, 1926, and 1931. The figures clearly show that no propagation exists below cutoff. However, there was a very small amount of the energy propagated in the form of numerical wave. We believe that the high frequency components which propagated are introduced by the discrete excitation.

We also simulated wave propagation in the presence of a discontinuity. A thin inductive metal strip was placed at the center of the waveguide WR-28. The wave propagation was observed at iteration numbers 100, 500, 800, 1000, 1200, and 1900, and the results are shown in Figs. 16(a)-(f), respectively. Due to the reflections from the discontinuity, we can see from Fig. 16 that it takes longer for the field to reach a steady state condition, than in the case without the discontinuity. Figures 16(a)-(f) illustrate the transmitted field distribution on the left hand side of the discontinuity and the total field distribution (the incident and reflected fields) on the right hand side of the discontinuity. Note that the SWR and S-parameters can be easily calculated from these field distributions.

We can observe pulse propgation phenomena in standard rectangular waveguide as well. A Gaussian pulse,

$$E_y(i, k) = e^{-\frac{k^2}{\omega^2}} \sin(\frac{\pi(i-1)}{NX}), \qquad (18)$$

is applied in the middle of the waveguide at time $t = 0$, where ω is the pulse width as shown in Fig. 17(a). As described in Section 2, we can see Fig. 17(b) that the incident pulse immediately splits into two pulses as illustrated in Fig. 17(c)-(g),
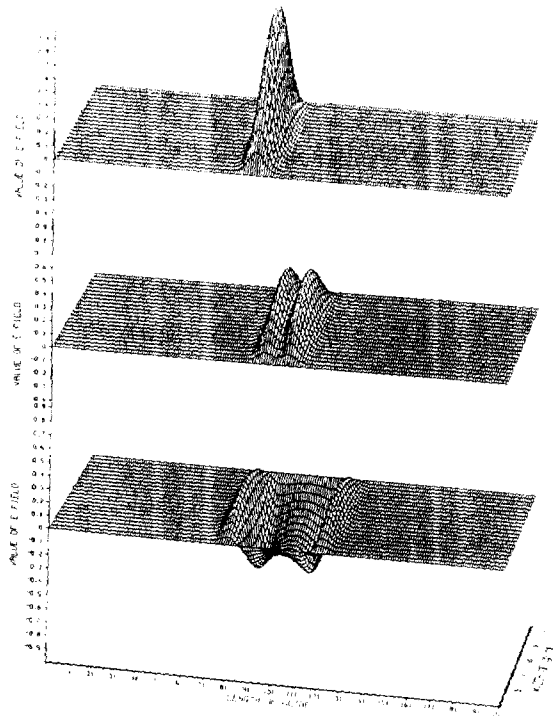
1607

Fig. 17. The numerical pulse wave propagation phenom
ena in a standard homogeneous rectangular
waveguide at iteration numbers (a)0, (b)5,
and (c)25. Excitation of a Gaussian pulse at
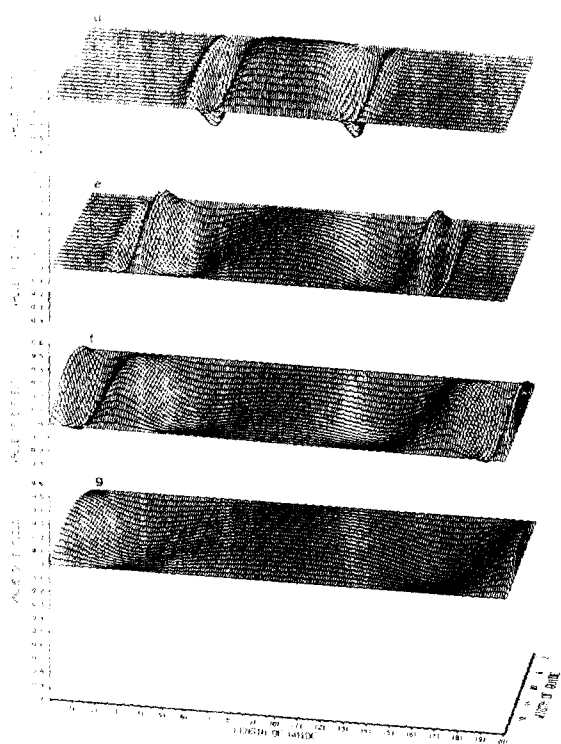the center of the waveguide.

Fig. 17. The numerical pulse wave propagation phenom
ena in a standard homogeneous rectangular
waveguide at iteration numbers (d)50, (e)100,
and (f)220

the two pulses continue to propagate in opposite
directions. This observation confirms that Max
well's equations describe two solutions propagat
ing in two opposite directions. Note that the pulse
width broadens as the wave propagates, since the
waveguide is dispersive. Figs. 17(h) and (i) use a
different scale, since almost all the energy has
been absorbed by the matching boundaries at the
right and left ends of the waveguide. Both the
higher frequency and lower frequency componen
ts below cutoff remain trapped in the computat
ional domain. which is especially obvious in Fig.
17(h) at iteration number 500, where we used an
amplitude scale one fourth of the scale in Fig. 17
(a). At iteration number 2500, (Fig. 17(i)), all the
higher frequency components have disappeared

since the higher frequency components propagate
slower than the lower frequency components (dis
persive nature). Only the components below cut
off remain stationary. For this case, 2500 itera
tions were sufficient to obtain an accurate fre
quency domain response through the Fourier tra
nsform. If a smaller number of iterations has
been used, we would have observed Gibbs phen
omenon.

Engineering parameters can be extracted from
the simulation of EM wave propagation phenom
ena. This has been done by calculating reflection
(S_{11}) and transmission coefficient with the FD
TD method. Following two examples shows the
accuracy of the FD TD method. Reflection prop
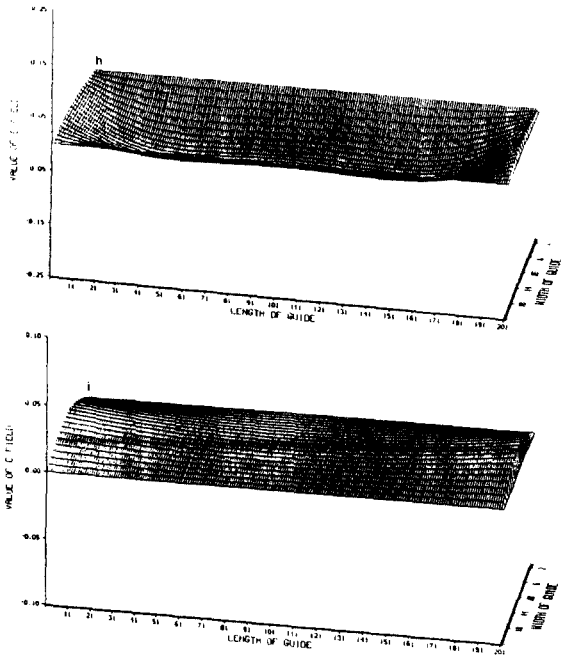erty of inductive irises in the WR 90 rectangula

Fig. 17. The numerical pulse wave propagation phenomena in a standard homogeneous rectangular waveguide at iteration numbers (h) 500, (i) 2500.

Fig. 18. S_{11} of symmetrical inductive irisee in WR-90.

waveguide is shown in Fig. 18. The FD-TD result is compared with TLM(Transmission Line Matrix) and a theoretical calculation, and shows good agreement with the other methods. The second example is shown in Fig. 19. Reflection and transmission properties are compared with well proven mode matching technique. Even though there is a little discrepencies in amplitude, there shows a good agreement in frequency characteristics.

Ⅶ. Conclusions

The numerical simulation properties of the FD-TD approach for EM wave propagation have been illustrated by using the analogy between the numerical and the analytical (continuous) characteristics of Maxwell's two time-dependent curl equations. This simulation method has been treated as a physical model, with which EM wave
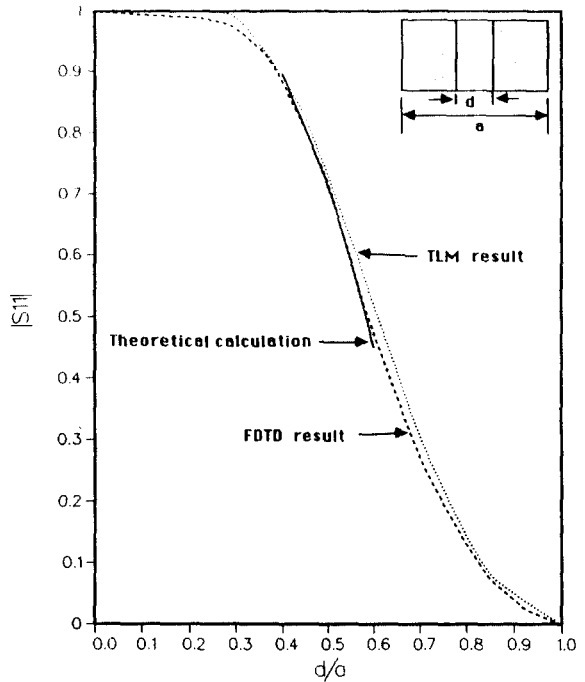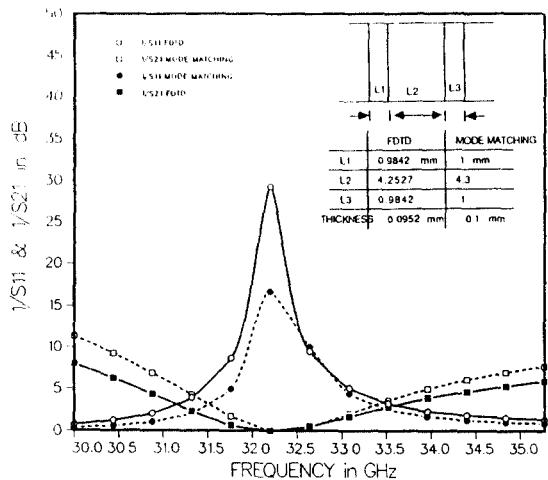

Fig. 19. One resonator E-plane filter characteristics in WR-28.

1609

propagation processes can be seen in a sequence of discrete events. The stability factor affecting the numerical wave propagation process has also been described in terms of the numerical wave velocity error (dispersion) which is directly related to the accuracy and economy of computation. The qualitative and quantitative observations of the numerical wave propagation in a rectangular waveguide illustrate the descriptive modeling ca pability of the FD-TD method. Thus, any experi mental work can be done with this numerical model without disturbing the field distribution through probing (sampling) of field quantities, and with great freedom in the selection of boundary conditions.

References

1. Ames, W.F., Numerical Methods for Partial Di fferential Equations, Academic Press, 1977.

2. Yee, K.S., "Numerical Solution of Initial Boun dary Value Problems Involving Maxwell's Equa tions in Isotropic Media", IEEE Trans. Ante nnas and Propagation, Vol. AP-14, No. 3, May 1966, pp. 302-307.

3. Taflove, A., and M.E. Brodwin, "Numerical Solution of Steady State Electromagnetic Sc attering Probrums Using the Time-Dependent Maxwell's Equations", IEEE Trans. Microwave Theory and Tech, Vol. MTT-32, No.8, Aug. 1975, pp. 623-630.

4. Holland, R., "THREDE:a Free-Field EMP Cou pling and Scattering Code", IEEE Trans. Nu clear Science, Vol. NS-24, No. 6, Dec. 1977, pp. 2416-2421.

5. Kunz, K.S. and K.M. Lee, "A Three-Dimens ional Finite Difference Solution of the External Response of an Aircraft to a Complex Transi ent EM Environment:Part 1 and Part 2", IEEE Trans. Electromagnetic Compatibility, Vol. EMC-20, No. 2, May 1978, pp. 328-341.

6. Taflove, A., "Application of the Finite-Differ ence Time-Domain Method to Sinusoidal Stea dy-State Electromagnetic-Penetration Proble ms", IEEE Trans. Electromagnetic Compati

7. Holland, R., L. Simpson, and K.S. Kunz, "Fi nite-Difference Analysis of EMP Coupling to Lossy Dielectric Structures", IEEE Trans. Electromagnetic Compatibility, Vol. EMC-22, No. 3, Aug. 1980, pp. 203-209.

8. Kunz, K.S., and H.G. Hudson, "Experimental Validation Of Time-Domain Three-Dimensional Finite-Difference Techniques For Predicting Interior Coupling Responses", IEEE Trans. El ectromagnetic Compatibility, Vol. EMC-28, No. 1, Feb. 1986, pp. 30-37.

9. Taflove, A., K. Umashankar, B. Beker, F. Har foush, and K.S. Yee, "Detailed FD-TD Analysis of Electromagnetic Fields Penetrating Narrow Slots and Lapped Joints in Thick Conducting Screen", IEEE Trans. Antenna and Propa., Vol. AP-36, No. 2, Feb. 1988, pp. 247-257.

10. Turner, C.D., and L.D. Bacon, "Evaluation of a Time-Slot Formalism for Finite-Difference Time-Domain Electromagnetics Codes", IEEE Trans. Electromagnetic Compatibility, Vol. EMC-30, No. 4, Nov. 1988, pp. 523-528.

11. Zhang, X., and K.K. Mei, "Time Domain Fi nite Difference Approach to the Calculation of the Frequency-Dependent Characteristics of Microstrip Discontinuities", IEEE Trans. Mi crowave Theory and Tech., Vol. MTT-36, No. 12, DEC. 1988, pp. 1775-1787.

12. Wang, C. Q., and O.P. Gandhi, "Time Domain Finite Difference Approach to the Calculation of the Frequency Dependent Characteristics of Microstrip Discontinuities", IEEE Trans. Microwave Theory and Tech., Vol. MTT-37, No. 1, Jan. 1989, pp. 118-125.

13. Liang, G.C., Y.W. Liu, and K.K. Mei, "Analysis of Coplanar Waveguide by the Time Domain Finite Difference Method", 1989 IEEE MTT-S International Symposium, pp. 1005-1008.

14. Courant, R., K.O. Friedrichs, and H. Lewy, "On the Partial Difference Equations of Math ematical Physics", (English translation from

the original appeared in Math. Ann., 100 (1928), pp.32-74), IBM Jour. Res. Devel., 11, 1967, pp. 215-234.

15. Mitchell, A.R., The Difference Methods in Partial Differential Equations, John Wiley and Sons, 1982.

16. Taflove, A, "Review of the Formulation and Applications of the Finite-Difference Time-Domain Method for Numerical Modeling of Electromagnetic Wave Interactions with Arbitrary Structures", Wave Motion, 10, 1988, pp. 547-582.

17. Kim, I.S., and W.J.R. Hoefer, "Effect of the Stability Factor on the Accuracy of Two-Dimensional TD-FD Simulation", 1989 IEEE AP-S Symposium Digest, pp. 1108-1111.

18. Kim, I.S., and W.J.R. Hoefer, "The Dispersion Characteristics and the Stability Factor of the TD-FD Method", Electronics Letters, April 1990, pp. 485-487.
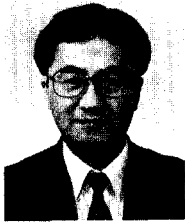
金 仁 爽(Ihn S. Kim)　　正會員
1947年 8月 4日生
1974년 2월 : 경희대 전파공학과(학사)
1980년 8월 : 한국방송공사 기술국 기술사원
1983년 2월 : Univ. of Ottawa(카나다), 전기공학과(석사)
1985년 8월 : General Instrument(카나다), Senior Engineer
1990년 10월 : Univ. of Ottawa(카나다), 전기공학과(박사)
1991년 2월 : Space Agency(카나다), David Florida Lab., Research Scientist
1994년 8월~현재 : 경희대학교 전자공학과 조교수

1611